REPORT R-420 JUNE, 1969

CSL COORDINATED SCIENCE LABORATORY

TUNNELING MEASUREMENT OF ELECTRON-PLASMON INTERACTIONS IN DEGENERATE SEMICONDUCTORS

C.B. DUKE
M.J. RICE
F. STEINRISSER

UNIVERSITY OF ILLINOIS - URBANA, ILLINOIS

This work was supported in part by the Joint Services Electronics Program (U.S. Army, U.S. Navy and U.S. Air Force) under Contract DAAB-07-67-C-0199, and in part by the National Aeronautics and Space Administration under contract NsG 228-62.

This report was also issued as Report No. 69-C-049 by the General Electric Research and Development Center in Schenectady, New York, January, 1969.

TUNNELING MEASUREMENT OF ELECTRON-PLASMON INTERACTIONS IN DEGENERATE SEMICONDUCTORS

C. B. Duke, M. J. Rice and F. Steinrisser

ABSTRACT

The electronic proper self energy due to electron-plasmon interactions in degenerate semiconductors has been evaluated using the Random Phase Approximation. This self energy together with elementary models of the barrier penetration factor is used to calculate the tunneling characteristics of rectifying metal contacts on the degenerate semiconductors. The calculations predict broad, doping-dependent resonances in d^2I/dV^2 at $|eV|$ approximately equal to the plasmon energy, $\hbar\omega_p$, in the semiconductor. In contrast to the analogous calculations for electron-phonon interactions, the major features of the predicted lineshapes are due to quasiparticle renormalization [i.e., $\underset{\sim}{k}$ dependence of the self energy] rather than quasiparticle dispersion [i.e., ε dependence of the self energy]. Comparison of the model calculations with experimental data taken using indium contacts on selenium and tellurium doped GaAs, $2.1 \times 10^{18} cm^{-3} \leq n \leq 6.2 \times 10^{18} cm^{-3}$, show satisfactory agreement between the predicted and observed lineshapes. The resonance structure in the experimental d^2I/dV^2 characteristics is identified independently with the plasmon energy in the GaAs electrode by correlation with the plasma minimum observed in the infrared reflectivity of the samples used in the tunneling measurements.

TUNNELING MEASUREMENT OF ELECTRON-PLASMON INTERACTIONS IN DEGENERATE SEMICONDUCTORS*

I. INTRODUCTION

In the past year, a comprehensive version of the transfer-Hamiltonian model of electron tunneling has been developed[1-3] which proves a quantitative basis for the extraction from tunneling experiments of information about the spectral density associated with collective excitations in the various components of a tunnel junction, and about their interaction with the tunneling electron. Within the framework of this model, two distinct mechanisms exist by which collective excitations can influence the tunneling characteristics. The simplest of these is the occurrence of an inelastic tunneling process in which the electron excites a collective mode "during" the tunneling process. Such processes occur in p-n tunnel diodes[4,5], Josephson junctions[6], metal-insulator-metal junctions[7,8], and metal-semiconductor contacts[9-11]. The second mechanism consists of electron-collective mode interactions in the electrodes[12] analogous to the case of electron interactions in the electrode leading to superconductivity[13]

The most extensively examined case of electron-collective-mode interactions is that of electron-phonon interactions[1-5,7-12,14,15]. The

---

*This work was supported in part by the National Aeronautics and Space Administration under Grant NsG 228-62, by the Joint Services Electronics Program, Army Contract DAAB-07-67-C-0199, and by the U.S. Army Research Office (Durham) under Contract DA-31-124-ARO(D)-114.

only other reported example is that of the interaction of electron pairs and electrons with cavity modes in tunnel junctions with superconducting electrodes[2,6]. In particular, the effects of electron-magnon interactions have been predicted[9] but not observed. In this paper we report the results of a study of a fourth example: the interaction between the tunneling electron and the plasma oscillations [plasmons] characteristic of the degenerate electron fluid in a heavily doped semiconductor. In particular, we calculate the tunneling characteristics for a model metal-semiconductor [or metal-oxide-semiconductor] junction and compare them with data taken using indium contacts on air-cleaved GaAs. Although the experiments are not completely definitive, our analysis leads us to interpret them as the first tunneling observation of electron-plasmon interactions. This interpretation is substantiated not only by the lineshape calculations, but also by the correlation of the plasma minimum in the infrared reflectivity curve with the observed resonant structure d^2I/dV^2 observed at 4.2 and $77^{o}K$ in units made on tellurium and selenium doped GaAs in the range $2.1\times10^{18}cm^{-3} \leq n \leq 6.2\times10^{18}cm^{-3}$.

Tunneling studies of the electron-plasmon interaction are of particular interest for several reasons. First, no confusion arises between the inelastic excitation of "barrier" modes and the mechanism of electron interactions in the electrodes. The plasmons are collective excitations characteristic only of the "electrode" portion of the semiconductor. Second, in contrast to the case of the polar interaction of electrons with LO phonons[16], in the random-phase-approximation (RPA) the

electron-plasmon interaction vertex for momentum transfer $\underset{\sim}{q}$ has the form $\underset{\sim}{q}^{-2}$ unaffected by screen considerations[17]. It is of interest to note that

$$r_s = \left(\frac{3}{4\pi n}\right)^{1/3} / a_B \tag{1.1a}$$

$$a_B = \epsilon_o \left(\frac{m}{m^*}\right) \quad (5.29\times10^{-9})\,\text{cm} \tag{1.1b}$$

assumes the values $r_s \sim 0.4$ for n-type GaAs in the doping range $2\times10^{18}\,\text{cm}^{-3} \leq n \leq 6\times10^{18}\,\text{cm}^{-3}$ if the values[14,18] $\epsilon_o = 13$, $m^* = 0.078\ m$ are used. Therefore we expect the RPA to be an acceptable approximation for these materials. The resulting strong $\underset{\sim}{q}$ dependence of the electron-plasmon interaction vertex causes the momentum dependence of the electronic proper self energy to make significant contributions to the lineshapes of the tunneling characteristics. Third, for the electron fluid in GaAs, $\zeta/\hbar\omega_p \sim 1.5$ where $\zeta = \hbar^2 k_F^2/2m^*, [k_F \equiv (3\pi^2 n)^{1/3}]$ is the Fermi energy and $\omega_p = (4\pi n e^2/\epsilon_o m^*)^{1/2}$ is the $\underset{\sim}{q}=0$ plasma frequency characterizing the electron fluid. Therefore, the dispersion of the plasmon energy with $\underset{\sim}{q}$ is substantial[19] and plays a significant role in determining the electronic self energy and hence the tunneling lineshapes. Finally, the maximum wave vector, q_o, for which a plasmon is defined satisfies[19,20]

$$\left[1 + \frac{q_o}{2k_F}\right] \ell n \left[\frac{q_o + 2k_F}{q_o}\right] = 1 + \frac{8}{3}\left(\frac{\zeta}{\hbar\omega_p}\right)^2 \left(\frac{q_o}{k_F}\right)^2 . \tag{1.2}$$

In the relevant doping range in GaAs, $q_o \cong (0.4)k_F$. This small value of q_o, the large plasmon dispersion, and small electron lifetimes [due to optical phonon emission when $\omega_{LO}<\omega_p$] conspire to give a weak structure in the predicted tunneling characteristics. An interesting feature of the lineshape calculation is the sensitivity of the results to the above four, relatively minute, aspects of the dynamic electron-plasmon interaction. This fact re-emphasizes the potential utility of tunneling spectroscopy as a probe of details in the many-body description of carriers in semiconductors which are inaccessible via conventional measurements of the bulk properties of the semiconductor.

The body of the paper is organized so that we present in sec. 2 a definition of the model electron-plasmon interaction and in sec. 3 the calculation of the model electronic self energy. In sec. 4 a calculation of zero-temperature lineshapes is given using some simple models of the one-electron barrier-penetration factor. The experimental results are presented in sec. 5 and compared with the model calculations. The paper concludes with a summary of the results, and a resumé of our main conclusions.

II. DEFINITION OF THE MODEL

The electronic self energy is calculated using the second-order perturbation-theory expression[13,17,20-23]

$$\Sigma(\underset{\sim}{k},i\epsilon_p) = -\frac{e^2\kappa T}{2\pi^2}\sum_{\omega_n}\int d^3q\,\frac{1}{q^2\epsilon(\underset{\sim}{q},\omega_n)}\,\mathcal{G}(\underset{\sim}{k}+\underset{\sim}{q},i\epsilon_p+i\omega_n) \qquad (2.1a)$$

$$\omega_n = 2\pi n/\varkappa T \tag{2.1b}$$

$$\epsilon_p = 2\pi(p+1)\ /\varkappa T \tag{2.1c}$$

in which n and p are integers; $\mathcal{G}(\underset{\sim}{k}, i\epsilon_p)$ denotes the one-electron propagator, and $[q^2\epsilon(\underset{\sim}{q},\omega_n)]^{-1}$ is the dynamically-screened electron-electron interaction. The notation follows that developed in ref. 23. In our calculation three major approximations are utilized in evaluating the sum and integral in Eq. (2.1a). First, the one electron propagator is taken to be the free-electron propagator

$$\mathcal{G}_o(\underset{\sim}{k}, i\epsilon) = [i\epsilon - \xi_{\underset{\sim}{k}}]^{-1} \tag{2.2a}$$

$$\xi_{\underset{\sim}{k}} = \frac{\hbar^2 k^2}{2m^*} - \zeta \tag{2.2b}$$

$$\zeta = \hbar^2 k_F^2/2m^* \tag{2.2c}$$

in the integrand. [However, we shall phenomenologically modify our final results to incorporate the effect of electron damping in the intermediate state due to electron-phonon and electron-impurity scattering.] Second, we use the random phase approximation[13,17,20-23] (RPA) for the dielectric screening function, and replace the (presumably) random distribution of positively charged donor ions by a uniform positive background[24,25]. The motivation for this approximation is our consideration only of electrons

injected into the (reverse-biased) semiconductor electrode at energies $E \gtrsim \zeta+\hbar\omega_p$. For such high-energy electrons, the impurity potentials act primarily as (screened) scattering centers[24]. Therefore, their major influence on the electronic self energy is to cause a finite lifetime which, as noted earlier, we shall incorporate together with the electron-phonon lifetime via a single phenomenological damping parameter, Γ. Our third approximation consists of writing

$$\frac{1}{\epsilon(\underset{\sim}{q},i\omega_n)} = 1 + \frac{1}{\epsilon(q,i\omega_n)} - 1 \qquad (2.3)$$

and retaining only the plasmon-pole contribution[17,20,26] to the bracketed quantity when performing the integral over $\underset{\sim}{q}$ in Eq. (2.1a). The motivation for this approximation is provided by the results of numerical calculations[26] of $\Sigma(\underset{\sim}{k},\epsilon)$ using the complete RPA form for $\epsilon(\underset{\sim}{q},i\omega_n)$ in the zero temperature ($T\to 0$) limit. These calculations show that the major contribution to $\mathrm{Im}\Sigma(\underset{\sim}{k},\epsilon)$ [and by inference all of the rapidly varying contributions to $\mathrm{Re}\Sigma(\underset{\sim}{k},\epsilon)$] for $k>k_F$ and $\epsilon\equiv(E-\zeta) \sim \hbar\omega_p$ result from the plasmon-pole contribution to Eq. (2.1a). The effects of the smaller, slowly varying contributions of the incoherent electron-hole excitations to $\Sigma(\underset{\sim}{k},\epsilon)$ [i.e. those resulting from the two cuts[16,20] in $\epsilon^{-1}(\underset{\sim}{k},i\omega_n)$] may be considered to be included in the phenomenological damping parameter.

The final consequences of the three approximations described above may be summarized conveniently by using a model electron-plasmon self energy defined by[17]

$$\Sigma_{p\ell}(\underset{\sim}{k},i\epsilon_p) = \frac{-e^2\hbar\omega_p\pi T}{\epsilon_\infty(2\pi)^2} \sum_{\omega_n} \frac{d^3q}{q^2} \mathcal{G}_0(\underset{\sim}{k+q},\ i\omega_n+i\epsilon_p)$$

$$F(q) \left[\frac{1}{i\omega_n-\hbar\omega(q)} - \frac{1}{i\omega_n+\hbar\omega(q)}\right] \tag{2.4}$$

in which $\omega(q)$ is the plasmon dispersion relation which we write in the form

$$\hbar\omega(q) = \hbar\omega_p + \alpha q^2 \tag{2.5}$$

and $F(q)$ is a function which is unity for small values of q and drops to nearly zero at a cut-off value, $q\equiv q_o$, defined[19,20] by Eq. (1.2). The value of α usually is evaluated by a small q expansion of the location of the zero of $\epsilon(q,\omega(q))$. We often shall use the value of α obtained by requiring that $\omega(q)$ is given by its exact value[19,20]

$$\frac{\omega(q)}{qv_F}\ \ell n\left[\frac{\omega(q)+qv_F}{\omega(q)-qv_F}\right] = \frac{8}{3}\left(\frac{\zeta}{\hbar\omega_p}\right)^2 \left(\frac{q}{k_F}\right)^2 + 2 \tag{2.6a}$$

$$v_F = \hbar k_F/m^* \tag{2.6b}$$

at $q=q_o$. This model approximation is convenient due to the large plasmon dispersion when r_s is small. We also use the model form

$$F(q) = \theta(q_o-q) \tag{2.7}$$

because this form is analytically convenient and involves essentially no error for long wavelength plasmons. Although we have neglected it, plasmon damping can be taken into consideration fairly simply[17].

We conclude this section by summarizing the distinctions between the model defined by Eqs. (2.4)-(2.7) and closely related calculations in the literature. It differs from the model of (unscreened) electron-LO-Phonon interactions analyzed by Mahan and Duke[16] (MD) because of (1) the finite cut-off wave-number q_o for the plasmons, (2) the occurrence of plasmon dispersion, and (3) the use of a phenomenological one-electron damping constant Γ due to electron-impurity and electron-phonon scattering. Hedin et al[26] extended the MD calculations to describe electron-plasmon interactions in metals by using a model electronic self energy similar to Eq. (2.4). Lundqvist[26] provided both an extensive numerical study of the consequences of their model, and a demonstration of that for $2 \lesssim r_s \lesssim 5$ the model provides an adequate approximation to the complete RPA self energy for $|\epsilon| \gtrsim \hbar\omega_p$. Our analysis differs from theirs via (1) the use of temperature rather than time-ordered Green's functions, (2) the investigation of a different range of density parameters, (3) the introduction of the phenonenological damping constant, and (4) the use of a finite plasmon cut-off wave number, q_o.

III. EVALUATION OF THE ELECTRONIC PROPER SELF ENERGY

Performing in the usual manner[2,23] the sum over ω_n in Eq. (2.4) gives our basic expressions for the retarded ($i\epsilon_p \to \epsilon + i\delta$) electronic self energy:

$$\Sigma_{p\ell}(\underset{\sim}{k},\epsilon) = \Sigma_+(\underset{\sim}{k},\epsilon) + \Sigma_-(\underset{\sim}{k},\epsilon) \tag{3.1a}$$

$$\Sigma_+(\underset{\sim}{k},\varepsilon) = g^2(k) \int_{-\zeta}^{\infty} d\xi_{\underset{\sim}{k}'} \int_{(k-k')^2}^{q_o^2} \frac{dx}{x} \frac{[N(\hbar\omega(x))+n(\xi_{k'})]}{\varepsilon - \xi_{\underset{\sim}{k}'} + \hbar\omega_p + \alpha x} \tag{3.1b}$$

$$\Sigma_-(\underset{\sim}{k},\varepsilon) = g^2(k) \int_{-\zeta}^{\infty} d\xi_{\underset{\sim}{k}'} \int_{(k-k')^2}^{q_o^2} \frac{dx}{x} \frac{[N(\hbar\omega(x))+n(\xi_{k'})}{\varepsilon - \xi_{\underset{\sim}{k}'} - \hbar\omega_p - \alpha x} \tag{3.1c}$$

$$N(y) = [\exp(y/\varkappa T)-1]^{-1} \tag{3.1d}$$

$$n(y) = [\exp(y/\varkappa T)+1]^{-1} \tag{3.1e}$$

$$g^2(k) = \frac{E_g}{2}\left(\frac{\hbar\omega_p}{\zeta}\right)\left(\frac{k_F}{k}\right) \tag{3.1f}$$

$$E_g = e^2 k_F/4\pi\varepsilon_\infty \tag{3.1g}$$

The upper limit of the x integration is defined as $\min\left\{q_o^2, (k+k')^2\right\}$. However, in the cases of interest to us $k>q_o$ so we have always used q_o^2 as the upper limit. For convenience, we also will use the $T\to 0$ limit of Eqs. (3.1) in which

$$N(y) \to 0 \tag{3.2a}$$

$$n(y) \to \theta(-y) \tag{3.2b}$$

The imaginary part of $\Sigma_{p\ell}$ may be calculated exactly from Eqs. (3.1) and the evaluation of the real part of $\Sigma_{p\ell}$ may be reduced to the (numerical) evaluation of a single quadrature. Some care must be taken in determining the integration regions which are shown in Fig. 1 for $\Sigma_-(k,\varepsilon)$ and in Fig. 2 for $\Sigma_+(\underset{\sim}{k},\varepsilon)$ in the $T\to 0$ limit. The imaginary part of the self energy is the line integral of $(\pi g^2/x)$ along the trajectory specified by

$$x_- = \gamma^{-1}[k_-^2(\varepsilon) - k'^2] \tag{3.3a}$$

$$k_-(\varepsilon) = \left\{\frac{2m^*}{h^2}\left[\varepsilon+\zeta-h\omega_p\right]\right\}^{1/2} \tag{3.3b}$$

$$\gamma = 2m^*\alpha/h^2 \tag{3.3c}$$

for $\sum_-$ and the trajectory specified by

$$x_+ = \gamma^{-1}[k'^2 - k_+^2(\varepsilon)] \tag{3.4a}$$

$$k_+(\varepsilon) = \left\{\frac{2m^*}{h^2}\left[e+\zeta+h\omega_p\right]\right\}^{1/2} \tag{3.4b}$$

for $\sum_+$. Two general properties of the electronic self energy are evident without detailed calculation. First, the weak-dispersion limit defined by $\gamma \to 0$ makes both trajectories vertical lines in the x-k'planes of Figs. 1 and 2 at $k' = k_{\pm}(\varepsilon)$ (independent of x). Second, the imaginary part of the self energy has a logarithmic singularity [and the real part a step discontinuity] when the $x_{\pm}(k',\varepsilon)$ trajectories pass through the pole of the integrand at x=0. Therefore these singularities occur at

$$k = k_+(\varepsilon) \quad ; \quad \sum_+(k,\varepsilon) \tag{3.5a}$$

$$k = k_-(\varepsilon) \quad ; \quad \sum_-(k,\varepsilon) \tag{3.5b}$$

for any value of γ. Note that this feature of the electronic self energy is a direct consequence of the $1/q^2$ behavior of the electron-plasmon interaction vertex.

The real part of the self energy at T=0 is obtained by numerical performance of the quadratures

$$\mathrm{Re}\Sigma_{+}(k,\epsilon) = g^2(k) \int_{E_{L+}(k)}^{E_{U+}(k)} d\xi_{k'}\, I_{+}(k,k',\epsilon) \tag{3.6a}$$

$$\mathrm{Re}\Sigma_{-}(k,\epsilon) = g^2(k) \int_{E_{L-}(k)}^{E_{U-}(k)} d\xi_{k'}\, I_{-}(k,k',\epsilon) \tag{3.6b}$$

$$I_{\pm}(k,k',\epsilon) = \frac{1}{\epsilon-\xi_{k'}\mp\hbar\omega_p} \ln \left[\frac{q_o^2}{(k-k')^2} \frac{\epsilon-\xi_{k'}\mp\hbar\omega(k-k')}{\epsilon-\xi_{k'}\mp\hbar\omega(q_o)} \right] \tag{3.6c}$$

The limits $E_{i\pm}(k)$ are determined from Figs. 1 and 2. They depend only on the value of k. Mahan and Duke[16] evaluated the integrals in Eqs. (3.6) analytically in the zero-dispersion limit that $\gamma \to 0$ so that

$$I_{\pm}(k,k',\epsilon) = \frac{1}{\epsilon-\xi_{k'}\mp\hbar\omega_p} \ln \left[\frac{q_o^2}{(k-k')^2} \right] \tag{3.7}$$

However, no cut-off was used in ref. 16 so that q_o^2 in Eq. (3.7) was replaced by $(k+k')^2$. A simple approximation, which is qualitatively correct provided k is not near k_F, is obtained by taking only the singular terms in the real self energy in the $\gamma \to 0$ limit, i.e.

$$\mathrm{Re}\Sigma_{sing}(k,\epsilon) = g^2(k) \ln \left[\frac{q_o^2}{(k-k_F)^2} \right] \theta\,(k_F+q_o-k)$$

$$\times\, \theta(k-k_F+q_o) \ln \left| \frac{\epsilon-\hbar\omega_p}{\epsilon+\hbar\omega_p} \right| \tag{3.8}$$

The use of Eq. (3.8) is a convenient approximation for evaluating tunneling lineshapes because it saves the computer time required to perform the integrals in Eqs. (3.6). It gives a qualitatively correct lineshape for $\epsilon \sim \hbar\omega_p$ and $\xi_{\underset{\sim}{k}} \sim \hbar\omega_p$ but concentrates too much spectral weight in the region of $\epsilon \cong \hbar\omega_p$ for a given value of $\underset{\sim}{k}$. A comparison of the $\gamma=0$ singular and exact real self energies is shown in Fig. 3. Also shown is the exact real self energy including the effects of plasmon dispersion for undamped plasmons described by the RPA. The large increase in $\mathrm{Re}\Sigma(\underset{\sim}{k},\epsilon)$ at $k=k_-(\epsilon)$, [associated with the divergence in $\mathrm{Im}\Sigma(\underset{\sim}{k},\epsilon)$ described by Eq. (3.5b)] is clearly evident in the numerically evaluated self energies.

In all of our numerical calculations we have incorporated the effect of electron-phonon and electron-impurity scattering by use of a phenomenological damping constant Γ which is roughly equal to the energy width of a one-electron state due to these scattering mechanisms. From studies of electron-phonon interactions in silicon[12], which produce effects at $eV \cong \hbar\omega_{LO}$ of roughly comparable magnitude to those observed in GaAs, we anticipate that $1\text{meV} \lesssim \Gamma \lesssim 10\text{meV}$. [In units of the plasma frequencies of interest in the experimental data to be shown later we expect $0.02 \lesssim (\Gamma/\hbar\omega_p) \lesssim 0.2$.] Much of this energy width may be due to phonon emission by the injected electron because $\hbar\omega_{LO} < \hbar\omega_p$. These results have the interesting consequence that in GaAs usually $\mathrm{Im}\Sigma_{p\ell} \cong 0.02\ \hbar\omega_p \lesssim \Gamma$. Therefore the additional damping which onsets when $|\epsilon| > \hbar\omega_p$ does not exert any substantial effect on the lineshapes of the tunneling characteristics.

The most rigorous approach to the evaluation of the effects on plasmon emission of phonon creation, incoherent electron-hole pair creation, and impurity scattering is to use an electron propagator $\mathcal{G}$ in Eq. (2.4) which contains a self-energy contribution due to these interaction mechanisms. However, in any such analysis approximations must be employed. Therefore, after studying the exact expressions for $\Sigma(\underset{\sim}{k},\epsilon)$ resulting from such an analysis we decided to adopt the purely phenomenological approach of replacing Eq. (3.6c) by

$$I_{\pm}(k,k',\epsilon;\Gamma) \equiv \frac{(\epsilon-\xi_{k'}\pm\hbar\omega_p)}{(\epsilon-\xi_{k'}\pm\hbar\omega_p)^2+\Gamma^2} \tag{3.9}$$

$$\times \left\{ \ell n \left[\frac{q_o^2}{(k-k')^2} \right] + \frac{1}{2} \ell n \left[\frac{[\epsilon-\xi_{k'}\pm\hbar\omega(k-k')]^2+\Gamma^2}{[\epsilon-\xi_{k'}\pm\hbar\omega(q)]^2+\Gamma^2} \right] \right\} .$$

As Mahan and Duke[16] discussed for the case of unscreened polar coupling to LO phonons, the $\ell n[q_o^2/(k-k')^2]$ factor in (3.9) leads to divergences in $\partial\Sigma(k,\epsilon)/\partial\xi_k$ as $\epsilon\to 0$. For electron-plasmon coupling these divergences are cancelled[26] by those in the exchange self energy associated with the factor of 1 outside the brackets in Eq. (2.3). The fact that our model of the self energy is inaccurate for small values of $|\epsilon| \ll \hbar\omega_p$ is of no importance because we are interested in describing tunneling lineshapes for which $|\epsilon| \sim \hbar\omega_p$. For convenience in numerical integrations we set $q_o^2 \to [q_o^2 + 2m^*\Gamma_o/\hbar^2]$ and $(k-k')^2 \to [(k-k')^2 + 2m^*\Gamma_o/\hbar^2]$ in those calculations in which we evaluate derivatives of the self energy. This substitution

eliminates the spurious divergence at $\epsilon \to 0$ but does not materially affect the lineshape for $\epsilon \sim \hbar\omega_p$ provided $\Gamma_o \ll \Gamma$. Unless otherwise specified, $\Gamma_o \equiv (0.01)\,\hbar\omega_p \ll \Gamma$. Finally, we note that if $\alpha q_o^2 \ll \Gamma$ the use of the phenomenological formula (3.9) for the self energy introduces some spurious reduction of $\partial\Sigma/\partial\xi_k$ near $\epsilon = \hbar\omega_p$. Therefore Eq. (3.9) is an adequate phenomenological form only in the limits of weak damping ($\Gamma \to 0$) and/or small dispersion $\Gamma \gtrsim \alpha q_o^2$.

IV. CALCULATION OF THE TUNNELING CHARACTERISTICS

If we adopt a model of the tunneling process in which the component, $\underset{\sim}{k}_{//}$, of the electronic momentum parallel to the plane of the junction is conserved during the tunneling transition across the metal-semiconductor interface, then for tunneling from a free-electron metal into a degenerate semiconductor the current density is given by[2]

$$j(V,T) = \frac{-ei}{\pi\hbar} \int_{-\infty}^{\infty} [n(\epsilon) - n(\epsilon+eV)\,d\epsilon \int_{-\zeta}^{\infty} \mathrm{Im}G(\underset{\sim}{\xi}_k, \epsilon)\,d\underset{\sim}{\xi}_k$$

$$\int \frac{d^2 k_{//}}{(2\pi)^2} D(\underset{\sim}{\xi}_k, \underset{\sim}{k}_{//}; \epsilon; eV). \qquad (4.1)$$

In model descriptions[14,27,28] of one-electron tunneling into GaAs, the facts that the barrier height (V_b) of the Schottky barrier is larger than one-half the energy gap ($V_b > E_G/2$) and that $\zeta > \hbar\omega_p$ lead to the necessity of explicitly incorporating the bias (V) dependence of the barrier-penetration

factor (D) into the calculation of the one-electron tunneling characteristics. However, we are interested in calculations of the tunneling characteristics only in a relatively narror energy range about $\epsilon \sim eV \sim \hbar\omega_p$. Therefore we shall adopt simple models of the barrier penetration factor which describe the one-electron lineshape only in the region $eV \cong -\hbar\omega_p$, but which permit us to perform the $\underset{\sim}{k}_{||}$ and ϵ integrations in an elementary fashion.

Two (equivalent) models for the barrier penetration factor adequately describe the "background" characteristics of data for $eV \sim -\hbar\omega_p$ taken using metal contacts on n-type GaAs. They are defined by:

$$D = \frac{D_o}{E_o} \frac{\hbar^2 k_{||}^2}{2m} \tag{4.2a}$$

$$D = \frac{D_o}{2E_o} (\xi_{\underset{\sim}{k}} + \zeta) \quad . \tag{4.2b}$$

Both models lead to

$$\int \frac{d^2 k_{||}}{(2\pi)^2} D(\xi_{\underset{\sim}{k}}, \underset{\sim}{k}_{||}) = \frac{D_o \rho}{2E_o} (\zeta + \xi_{\underset{\sim}{k}})^2 \tag{4.3a}$$

$$\rho_{||} = m^*/2\pi\hbar^2 \tag{4.3b}$$

in which D_o is the barrier penetration factor of an electron at the fermi energy for $V \equiv 0$, and E_o is a quantity with units of energy, $E_o \sim \hbar\omega_p/2$. Using this model for D, the conductance at zero temperature is given by

$$G(V) \equiv dj/dV = \frac{-e^2 i}{2\pi h} \frac{\rho_{||} D_o}{E_o} \int_{-\zeta}^{\infty} (\zeta+\xi_k)^2 \; \mathrm{Im}G(\underset{\sim}{\xi_k}, -eV) d\underset{\sim}{\xi_k} \quad . \qquad (4.4)$$

By virtue of our model for $G(\underset{\sim}{\xi_k},\epsilon)$ developed in Sec. 3 we obtain

$$\mathrm{Im}\; G(\underset{\sim}{\xi_k},-eV) = \frac{[\mathrm{Im}\Sigma(\xi_k,-eV)-i\Gamma]}{[-eV-\xi_k-\mathrm{Re}\Sigma(\xi_k,-eV)]^2+[\Gamma+|\mathrm{Im}\Sigma(\xi_k,-eV)|]^2} \quad . \qquad (4.5)$$

The use of Eq. (4.5) in Eq. (4.3) can be greatly simplified by noting several general features of the parameter values of interest in our analysis of tunneling into GaAs. First, usually $\Gamma \gtrsim \mathrm{Im}\Sigma(\xi_k,-eV)$ so that the onset of plasmon emission for $eV<-\hbar\omega_p$ has little direct effect on ImG. Second, $\Gamma<<(\zeta+\hbar\omega_p)$ so that ImG is rapidly varying relative to the remainder of the integrand in Eq. (4.4). These two observations suggest the use of the quasi-particle approximation

$$\mathrm{Im}G(\xi_k,\epsilon) = \pi Z(\epsilon)\delta[\xi_k-\xi_o(\epsilon)] \qquad (4.6a)$$

$$\epsilon-\xi_o(\epsilon)-\mathrm{Re}\Sigma(\xi_o(\epsilon),\epsilon) = 0 \qquad (4.6b)$$

$$Z(\epsilon) = [1+\partial\mathrm{Re}\Sigma(\xi_k,\epsilon)/\partial\xi_k]_{\xi_k=\xi_o(\epsilon)} \qquad (4.6c)$$

in the evaluation of the integral in Eq. (4.4). This approximation leads to the simple result

$$G(V) = G_o Z(-eV)[\zeta+\xi_o(-eV)]^2/(\hbar\omega_p)^2 \qquad (4.7a)$$

$$G_o = e^2 \rho_{||} D_o(\hbar\omega_p)^2/2hE_o \quad . \tag{4.7b}$$

The accuracy of the quasiparticle approximation was checked by numerical integration of Eq. (4.4) and found to be within a few percent of the exact value for $\Gamma \gtrsim 0.1\ \hbar\omega_p$.

A major result of studies[2,12,14,16] of electron-phonon self-energy effects on the tunneling characteristics has been the observation that the factor Z(-eV) in Eq. (4.7) plays a relatively minor role in determining the model lineshapes because the dependence of $\Sigma(\underset{\sim}{\xi}_k,\epsilon)$ on $\underset{\sim}{\xi}_k$ is weak. Precisely the converse is the case for our model of electron-plasmon interactions. This prediction is illustrated by Fig. 4 in which the consequences of the quasiparticle approximation in the weak-damping, zero-dispersion limit are presented. The change in sign of the effect on the conductance due to quasiparticle renormalization [i.e. Z(-eV)] and that due to quasiparticle dispersion [i.e. $\xi_o(-eV) \neq -eV$] has been noted previously[2,14]. For polar electron interactions with LO phonons, screening of the interaction vertex has been claimed[14] to eliminate the dominance of the bias dependence of Z(-eV) over that of $[\xi_o(-eV)-eV]$. In the plasmon case, however, this vertex is known[17] to have a q^{-2} dependence in the RPA. The substantial change in the characteristics of the reverse-bias lineshapes at $eV \cong -\hbar\omega_p$ due to the q-dependence of the vertex is evident from Fig. 4.

For the parameters characterizing degenerate, n-type GaAs two additional aspects of the analyses exert a substantial effect on the

lineshapes. First, the large electron-phonon damping which is expected occur because $\hbar\omega_{LO} < \hbar\omega_p$ in the relatively heavily-doped tunneling units completely eliminates the cusp-like minimum in G(V). This effect is illustrated in Fig. 5 in which dG/dV is shown for the singular-self energy, zero-dispersion case the use of which has characterized the analyses[2,12,14,16] of electron-phonon coupling. In this figure the value of $\mathrm{Im}\Sigma[\xi_o(-eV),-eV]$ also is shown to illustrate that it is substantially smaller than Γ for those values of Γ which are expected to describe damping due to the electron-optical-phonon interactions. The second aspect of the analysis which affects the lineshape is the large amount of plasmon dispersion. We see from Fig. 3 that this dispersion removes the cusp in $\mathrm{Re}\Sigma(\underset{\sim}{\xi}_k,\epsilon)$ at $\epsilon=\hbar\omega_p$. This removal smears out the structure in both G(V) and dG/dV near $eV=\hbar\omega_p$. In particular, smaller values of Γ give smoother lineshapes with the minimum in Z(-eV) occurring for -eV of the order of $\hbar\omega_p+\alpha q_o^2$. The effects of using the complete self energy, given by Eqs. (3.6) and (3.9) are illustrated in Fig. 6 for the weak damping limit.

V. COMPARISON WITH EXPERIMENT

A. Experimental Details

GaAs samples were cut from single crystal material[29]. The sample size was 10 x 2.5 x 0.6 mm. The crystal was oriented such that a (110) cleavage surface was produced by breaking the bar in the middle. Ohmic contacts were made by soldering a nickel wire with an indium/lead solder containing 2% tellurium in a H_2-atmosphere to the GaAs. Conductance curves

run at 4.2°K with samples which had two such contacts indicated that such samples were ohmic and had a very low resistance.

Tunneling contacts were made by cleaving the samples in a vacuum of 1×10^{-7} torr or in air and by evaporating indium dots of 2.5×10^{-4} cm^2 area through a stainless steel mask. The evaporation of 99.999% pure indium from alumina coated tungsten wire baskets was begun about one minute before cleavage to stabilize the evaporation rate at 50 Å/sec. Cleavage was performed by a swinging hammer. The mask was brought close to the (110) cleavage surface, and a shutter between evaporation source and sample was opened until 5000 Å of indium were deposited. A quartz crystal deposition thickness monitor was used to measure rates and total film thickness. Electrical contacts to the indium dots were made by pressing a freshly cut indium tip into a dot located on a good cleavage plane.

The occurrence of tunneling was inferred from the observation of the BCS energy gap in indium below 3.4°K. The gap was seen in all junctions.

Barrier heights V_b between metal and semiconductor were determined by measuring capacitance C vs bias V at 77°K. A Boonton 33A rf admittance bridge was used. The modulation frequency was 1 MHz, the signal amplitude 5 mV. Plots of $1/C^2$ vs V gave straight lines whose intersection with the V-axis gave the value $V_b + 3/5\ \zeta$. The values of V_b for vacuum cleaved samples was 1.05 ± 0.05 eV, for air cleaved ones 0.80 ± 0.05 eV. Air cleavage gave larger junction conductance due to the lower barrier and was used for all but the highest doping levels. The detailed shape of d^2I/dV^2

curves, however, was the same for air and vacuum cleaved junctions.

Conductance $\left(dI/dV \right)$ and d^2I/dV^2 tunneling characteristics were measured with commonly used techniques[30]. The setup is basically the same as the one described in Figure 6 of Reference 30. A small ($\leq$ 2mV) ac bias voltage V_{ac} of frequency f = 1000 cps is superimposed on the dc bias. This bias is applied to the tunneling sample through a sampling resistor R which is equivalent to R_d in Figure 6 of Reference 30. The ac voltage developed across R is proportional to the ac current. It is picked up by a transformer T through large capacitors. This avoids passing dc current through the transformer. The signal picked up by the transformer T is detected by a lock-in amplifier.

The values of dI/dV and d^2I/dV^2 are related to the ac current flowing through the sampling resistor R at the frequencies f and 2f, respectively, by formulas (3) and (4) of Reference 30:

$$I(f) = \frac{dI}{dV}\left(1 + \frac{dI}{dV} \cdot R\right)^{-1} \cdot V_{ac} + \text{const.} \cdot \frac{d^3I}{dV^3} \cdot V_{ac}^{\,3} \tag{5.1}$$

$$I(2f) = 2^{-3/2} \cdot \frac{d^2I}{dV^2}\left(1 + \frac{dI}{dV} \cdot R\right)^{-3} \cdot V_{ac}^{\,2} + \text{const.} \cdot \frac{d^4I}{dV^4} \cdot V_{ac}^{\,4} \tag{5.2}$$

For $(dI/dV) \cdot R \ll 1$ and for negligible higher order terms, the output of the lock-in amplifier at the frequencies f and 2f is proportional to dI/dV and

d^2I/dV^2, respectively.

Curves of I(2f) (solid lines) and d^2I/dV^2 [solid lines for curves (4) and (5), dotted lines for curves (1), (2), and (3)] taken at 4.2°K are displayed in Figure 7. Positive bias values correspond to GaAs positive (reverse bias). The dotted lines in Figure 7 (corrected d^2I/dV^2 curves) were obtained by multiplying point by point the values of I(2f) by $[1 + (dI/dV)\cdot R]^3$ according to Eq. (5.2). The corrected values were normalized at a reverse bias of 50 mV. For curves (4) and (5), the corrections are very small. The term $(d^2I/dV^2\cdot V_{ac}{}^4$ is negligible for all curves.

The doping levels in the samples whose characteristics are displayed in Figure 6 were 6.2 x $10^{18}/cm^3$ (1), 4.2 x $10^{18}/cm^3$ (2), 4.1 x $10^{18}/cm^3$ (3), 3.5 x $10^{18}/cm^3$ (4), and 2.1 x $10^{18}/cm^3$ (5). The dopant was Te except for sample (3) where it was Se. Doping levels were obtained from a list of the position of the infrared (IR) reflectivity minimum vs. doping[31]. Reflectivity measurements were performed at room temperature on the samples used for tunneling measurements. A Perkin Elmer 521 grating IR spectrometer with a reflectance attachment was used. Arrows in Figure 7 denote the energy of the IR reflectivity minimum. The error in determining this energy is less than 2%. The reflectivity vs. wave length curves are very similar to those found in the literature[32]. The identification of a broad, doping-dependent inflection point[33] in d^2I/dV^2 with the plasma minimum in the reflectivity is evident from the figure. This identification together with the similarity of the observed line shape with the results of calculations

for reasonable values of the phonon and impurity induced level width, Γ [see, e.g. Figs. 5,6] provide strong evidence that the data shown in Fig. 7 may be interpreted in terms of plasmon-induced electronic self energy effects in the GaAs electrode.

B. Interpretation of the Data:

The sharp, doping-independent, resonances in d^2I/dV^2 at $eV \cong \pm$ (34-38) meV are attributed to the interaction of the electrons with optical phonons[14,34]. An analysis of this structure is complicated greatly both by the $\underset{\sim}{q}$ dependence of the screened polar-LO phonon vertex[16] and by the reduction of the difference between the LO and TO phonon energies near $k = 0$ in highly degenerate semiconductors[16,35] for which $\omega_p \gtrsim \omega_{LO}$. Thus we have not considered further the detailed interpretation of the phonon-induced resonances.

In sec. 4 we have discussed in some detail the plasmon-induced structure in reverse bias near $eV = -\hbar\omega_p$. The corresponding structure in forward bias is too indistinct to attempt to analyze. In addition, our model of the barrier-penetration factor [sec. 4] is inadequate in this region of the bias[2,14,27,28] and the impurities may exert a complex effect on the electronic energy spectrum. The major characteristics of the reverse-bias lineshape are (1) a distinct reduction in slope for values of the bias well below the plasma-reflectivity minimum (and hence $\hbar\omega_p$); (2) the broad character of the resonance structure, and (3) the generally weak nature of the resonance. From sec. 4, Figs. 4 and 5, we see that characteristic (1) is a consequence of the quasiparticle

renormalization factor, Z(-eV), due primarily to the q^{-2} dependence of the electron-plasmon vertex. Characteristics (2) and (3) are primarily consequences of the substantial electron-phonon and electron-impurity damping. However, they also are consequences of the generally weak nature of the electron-plasmon coupling [i.e. $E_g = e^2 k_F / 4\pi\epsilon_\infty \sim 0.07\ \hbar\omega_p$] and the strong plasmon dispersion.

In contrast to the case of electron-phonon interaction in homopolar semiconductors[12,36] a quantitative theoretical analysis of the experimental electron-plasmon interaction resonance in the reverse-bias tunneling characteristics seems unwarranted at the present time. First, in the more highly doped samples corrections to the experimental I(2f) curves are large in the region of this resonance. However, in the lower-doped samples, the plasmon-phonon interaction[37-41] is still significant but has not been incorporated into our model. We also have used a rough, completely phenomenological, treatment of electron damping due to phonon emission and impurity scattering. It is probably inadequate for a quantitative description of these processes in the strong-damping limit needed to describe the "hot" electrons injected near the plasmon energy. Finally, in our model we have neglected the damping of the plasmons themselves due to both electron-hole pair(s) excitation and impurity scattering. This neglect is partially responsible for the larger effect of plasmon dispersion predicted theoretically [in the low-damping limit, see Fig. 6] than that observed in the experimental line-shapes [Fig. 7]. These three "technical" deficiencies in our model of

the reverse-bias lineshapes, plus the improved treatment of both the barrier-penetration factor and the electron-impurity interactions required to describe the forward bias lineshape, indicate that a qualitative description of the major features of the experimental lineshapes is all that could be expected using our model. However, a comparison of Fig. 7 with Figs. 5 and 6 demonstrates that such a qualitative description is an immediate consequence of our analysis.

It should be emphasized that the model calculation involves only a single adjustable parameter (Γ) whose values are constrained to be in general agreement [1 meV $\lesssim \Gamma \lesssim$ 5meV] with magnitude of the broadening parameter [$\tau \cong 10^{-13}$ sec] used in analyses of the Raman[39,40] and infrared[41] spectroscopy of light scattering from the coupled plasmon-LO-phonon system. In the calculation we consistently used the value 13 for the dielectric constant because we did not include electron-phonon interactions in the model to reduce ϵ to its dynamic value[39] of ϵ_∞=11.3 when $\omega \gg \omega_{LO}$. This change would cause essentially no modification of the predicted lineshapes if Γ were increased commensurately with ϵ^{-1}.

VI. SUMMARY AND CONCLUSIONS

In secs. 2-3 a model description of the plasmon-pole contribution to the screened coulomb exchange electronic self energy in a degenerate semiconductor is developed. In sec. 4 this model is used to evaluate the tunneling lineshapes for a rectifying metal-semiconductor

contact described by a simple barrier penetration factor whose functional form was chosen to simulate the general characteristics exhibited by experimental data. In sec. 5 experimental measurements for n-type GaAs are presented whose qualitative features near $eV = -\hbar\omega_p$ are described adequately by the model calculation. The adequacy of this model description and the independent correlation of the hypothesized plasmon induced "resonance" structure in the tunneling measurements of d^2I/dV^2 with the plasma minimum observed in the infrared reflectivity lead us to identify this resonance structure with plasmon-induced modifications of the electronic self energy in the GaAs electrode portion of the metal-semiconductor contact. This data and its proposed interpretation constitute the first[2] reported observation of bulk plasmon-induced features of the tunneling characteristics in any type of tunnel junction. The observation of the "Josephson" plasma resonance, which is a junction effect due to an oscillatory charging of the two metal electrodes, has been reported[42] for thin metal-insulator-metal tunnel junctions.

A list of the deficiencies of the model developed in secs. 2 and 4 has been already given in sec. 5B. Their combined effects render the model description of the experimental data of a qualitative rather than a quantitative nature. However, our calculations constitute the first investigation of the influence on tunneling lineshapes due to electronic self-energy changes[2] both of the deviation of the energy spectrum of the intermediate boson from a straight line [i.e. our zero-dispersion limit] and of a strong momentum dependence of the electron-boson interaction

vertex. Therefore, these calculations describe the predictions of models which differ in these qualitative features from previous model descriptions of tunneling experiments, and hence should prove useful beyond their immediate application to the description of the experiments made using metal contacts on GaAs. The extension of the analysis of electron-plasmon interactions given above, and of electron-LO-phonon interactions given in ref. 35, to provide a quantitative rather than qualitative description of tunneling measurements on degenerate, polar semiconductors requires a thorough analyses in the RPA of the interacting electron-LO-phonon system[13,42], and a more careful consideration of the influence of impurities on the degenerate electron fluid[24].

In the experimental work presented in sec. 5 n-type GaAs was used as the semiconductor electrode. It is of interest to know in which other semiconductor electrodes either of the following conditions would be satisfied: (a) $\hbar\omega_p > \zeta$ and (b) $\hbar\omega_p < \hbar\omega_{LO}$. In case (a) it clearly will not be possible for an electron at the fermi surface in the semiconductor electrode to fill, by emitting a plasmon, a vacant hole left by a tunneling electron. Thus for $\hbar\omega_p > \zeta$ we expect to observe no resonant structure in the tunneling lineshape due to electron-plasmon interaction at forward bias. In case (b) the phenomenological damping parameter Γ will be small for bias voltage magnitudes smaller than $(\hbar\omega_{LO}/e)$. Therefore, if the impurity scattering is not prohibitively large we expect marked structure in the tunneling characteristics in accordance with the theoretical predictions of sec. 4. In order to

realize condition (a) we need a large effective mass and a small dielectric constant ($\hbar\omega_p/\zeta \sim m^*/m\epsilon$) together with a carrier density n within the practical doping range for a tunnel junction. Some possible systems are p- GaAs, n- PdTe and p- GaP with $n \lesssim 1.0\times10^{19}\,cm^{-3}$, and p- InSb with $n \lesssim 1\times10^{18}\,cm^{-3}$. Condition (b) will be satisfied for the same semiconductors if the latter mentioned values of n are reduced by a factor of two or more.

Summarizing, the model calculation of secs. 2-4 adequately describe qualitative features of the experimental data on n-type GaAs reported in sec. 5. The model also predicts qualitative changes in the line shape when $\hbar\omega_p > \zeta$ and $\hbar\omega_{LO}$. These changes might be observed, for example, using rectifying contacts on the semiconductors mentioned above.

ACKNOWLEDGEMENT

We would like to acknowledge the support and encouragement of W.D. Compton and to thank L. Schein for assistance in measuring barrier heights.

References

1. C.B. Duke in "Tunneling Phenomena in Solids", E. Burstein, ed., (Plenum Publishing Co., New York, 1969) chpt. 28.

2. C.B. Duke, Tunneling in Solids (Academic Press, New York, 1969) chpt. 7.

3. A.J. Bennett, C.B. Duke, and S.D. Silverstein, Phys. Rev., 176, (1968).

4. N. Holonyak, Jr., I.A. Lesk, R.N. Hall, J.J. Tiemann, and H. Ehrenreich, Phys. Rev. Letters 3, 167 (1959).

5. L. Esaki and Y. Miyahara, Solid State Electron 1, 13 (1960).

6. D.N. Langenberg, D.J. Scalapino, and B.N. Taylor, Proc. IEEE 54, 560 (1966).

7. J. Lambe and R.C. Jaklevic, Phys. Rev. 165, 821 (1968).

8. I. Giaever and H.R. Zeller, Phys. Rev. Letters 21, 1385 (1968).

9. C.B. Duke, S.D. Silverstein, and A.J. Bennett, Phys. Rev. Letters 19, 312 (1967).

10. F. Steinrisser, L.C. Davis, and C.B. Duke, Phys. Rev., 176, (1968).

11. P. Thomas and H.J. Queisser, Phys. Rev., 175, 983, (1968).

12. L.C. Davis and C.B. Duke, Solid State Comm. 6, 193 (1968).

13. J.R. Schrieffer, Theory of Superconductivity (W.A. Benjamin, Inc., New York, 1964).

14. J.W. Conley and G.D. Mahan, Phys. Rev. 161, 681 (1967).

15. E.L. Wolf, Phys. Rev. Letters 20, 204 (1968).

16. G.D. Mahan and C.B. Duke, Phys. Rev. 149, 705 (1966).

17. D.F. DuBois, Ann. Phys. (N.Y.) 8, 24 (1959); 7, 174 (1959).

18. P.A. Schuman, Jr., and R.A. Phillips, Solid State Electron 10, 943 (1967).

19. R.A. Ferell, Phys. Rev. 107, 450 (1957).

20. S.M. Bose, A. Bardasis, A.J. Glick, D. Hone, and P. Longe, Phys. Rev. 155, 379 (1967).

21. J.J. Quinn and R.A. Ferrell, Phys. Rev. 112, 812 (1958).

22. J.J. Quinn, Phys. Rev. 126, 1453 (1962).

23. A.A. Abrikosov, L.P. Gorkov, and I.E. Dzyaloshinski, Methods of Quantum Field Theory in Statistical Physics (Prentice Hall, Inc., Englewood Cliffs, 1963), sec. 22.

24. P.A. Wolff, Phys. Rev. 126, 405 (1962).

25. J.S. Langer, Phys. Rev. 124, 1003 (1961).

26. L. Hedin, B.I. Lundqvist, and S. Lundqvist, Solid State Comm. 5, 237 (1967): B.I. Lundqvist, Phys. Kondens. Materie, 6 193 (1967); 6 206 (1967); 7, 117 (1968).

27. F.A. Padavoni and R. Stratton, Phys. Rev. Letters 16, 1202 (1966).

28. R.A. Stratton and F.A. Padovani, Solid State Electron, 10, 813 (1967).

29. We are indebted to Prof. N. Holonyak, Jr., and to the Monsanto Company for supplying GaAs samples. We wish to thank J. Rossi for help with many aspects of sample preparation.

30. R.T. Payne, Phys. Rev. 139, A570 (1965).

31. K. Okada and T. Oku, Japan. J. Appl. Phys. 6, 276 (1967).

32. W.G. Spitzer and J.M. Whelan, Phys. Rev. 114, 59 (1959).

33. Also using metallic contacts on n- GaAs, M. Mikkov and W.C. Vassel (Scientific Laboratory, Ford Motor Company) have discovered similar resonant structure in d^2I/dV^2. We are grateful to J. Lambe for bringing this work to our attention.

34. D.C. Tsui, Phys. Rev. Letters 21, 994 (1968).

35. R.A. Cowley and G. Dolling, Phys. Rev. Letters 14, 549 (1965).

36. L.C. Davis and C.B. Duke, to be published.

37. B.B. Varga, Phys. Rev. 137, A1896 (1965).

38. A. Mooradian and G.B. Wright, Phys. Rev. Letters 16, 999 (1966).

39. A. Mooradian and A.L. McWhorter, Phys. Rev. Letters 19, 849 (1967).

40. B. Tell and R.J. Martin, Phys. Rev. 167, 381 (1968).

41. C.G. Olson and D.W. Lynch, Phys. Rev. (to be published).

42. A.J. Dahm, A. Denestein, T.F. Finnegan, D.N. Langenberg, and D.J. Scalapino, Phys. Rev. Letters 20, 859 (1968).

43. A. Ron, Phys. Rev. 132, 978 (1963).

Figure 1 - The shaded region indicates the integration region of the k'-x plane relevant for the evaluation of $\Sigma_-(\underset{\sim}{k},\epsilon)$, given by Eq.(3.1c) in the text, when T=0. Figure 1(a) illustrates the case of $k>(k_F+q_o)$ and Figure 1(b) illustrates the case of $k<(k_F+q_o)$.

Figure 2 - The shaded region indicates the integration region of the k'-x plane relevant for the evaluation of $\Sigma_+(\underset{\sim}{k},\epsilon)$, given by Eq. (3.1b) in the text, when T=0. Figure 2(a) illustrates the case of $(k_F-q_o)<k<(k_F+q_o)$ and Figure 2(b) illustrates the case of $q_o<k<(k_F-q_o)$. The case that $k<q_o$ is more complicated because q_o^2 is no longer the upper limit of the x integral, but rather $\min[q_o^2,(k-k')^2]$ is this upper limit.

Figure 3 - Plots of the real self energy for $\xi_k=\hbar\omega_p$ as a function of ϵ, using a small damping parameter $\Gamma=0.01\ \hbar\omega_p$, and values of the material constants appropriate for a n-type doping of $2.1 \times 10^{18}\text{cm}^{-3}$ in GaAs. The solid line denotes the self energy calculated numerically from Eqs.(3.6) and (3.9). The dashed line denotes the self energy obtained by setting $\alpha\equiv 0$ in Eq.(3.9). The dot-dashed line is the singular contribution to the self energy obtained by setting $\epsilon \rightarrow [\epsilon^2+\Gamma^2]^{\frac{1}{2}}$ in Eq.(3.8). The accuracy of the numerical integrations is $\pm 3\%$. The rounding parameter Γ_o was taken to be $\Gamma_o=0.001\ \hbar\omega_p$. [See discussion following Eq.(3.9).]

Figure 4 - Various forms of the tunnel conductance obtained from Eqs.(4.7) in the text using parameters suitable for the GaAs with a doping of $n=2.1\times10^{18}cm^{-3}$. The zero-dispersion, singular self energy given by Eq.(3.8) was used in the calculation. The solid line shows the prediction of Eq.(4.7a) whereas the dashed line shows this prediction if $Z\equiv1$. The dot-dashed line gives the one-electron conductance obtained if $\Sigma_{p\ell}(\underset{\sim}{k},\epsilon)\equiv0$.

Figure 5 - The three continuous curves are associated with the left hand scale and represent $d[G(V)/G_o]/d(eV)$ calculated from Eqs.(3.8), (3.9), and (4.7) in the text. The insert in the lower right hand corner is the imaginary part of the energy-shell self energy, $iIm\Sigma[\xi_o(-eV),-eV]$, evaluated for $\Gamma\equiv0$, $\alpha\equiv0$ from Eqs.(3.1) in the text.

Figure 6 - Plots of the tunnel conductance in the weak-damping limit obtained using the complete electronic self energy specified by Eqs. (3.6) and (3.9) in the text using $\Gamma_o=\Gamma/10$. The solid line denotes the conductance obtained using Eqs.(3.6), (3.9) and (4.7) in the text with parameters appropriate for $n=2.1\times10^{18}cm^{-3}$ in GaAs. The dashed line shows the same calculation neglecting plasmon dispersion [i.e., setting $\alpha\equiv0$ in Eq.(3.9)]. The dot-dashed line shows the conductance obtained when α is set equal to one-fourth of the RPA value. The dashed line and dot-dashed lines are shifted by two and four units respectively above the solid line for ease in visualization.

Figure 7 - Structure in d^2I/dV^2 of indium contacts on n-type GaAs at 4.2°K. Solid lines represent the measured values of I(2f). Dotted lines are obtained from I(2f) by application of a correction factor mentioned in the text. They represent d^2I/dV^2 values, as do the solid curves (4) and (5) for which the corrections are negligible. The doping levels are $6.2 \times 10^{18}/cm^3$(1), $4.2 \times 10^{18}/cm^3$(2), $4.1 \times 10^{18}/cm^3$(3), $3.5 \times 10^{18}/cm^3$(4), and $2.1 \times 10^{18}/cm^3$(5). The dopant is Te except for sample (3) where it is Se. Arrows indicate the position of the infrared reflectivity minima measured on the tunneling samples at room temperature. The relation between the plasma frequency and the location of the reflectivity minimum is not defined precisely because no analysis of the reflectivity lineshapes was undertaken [see, e.g., Ref. 41].

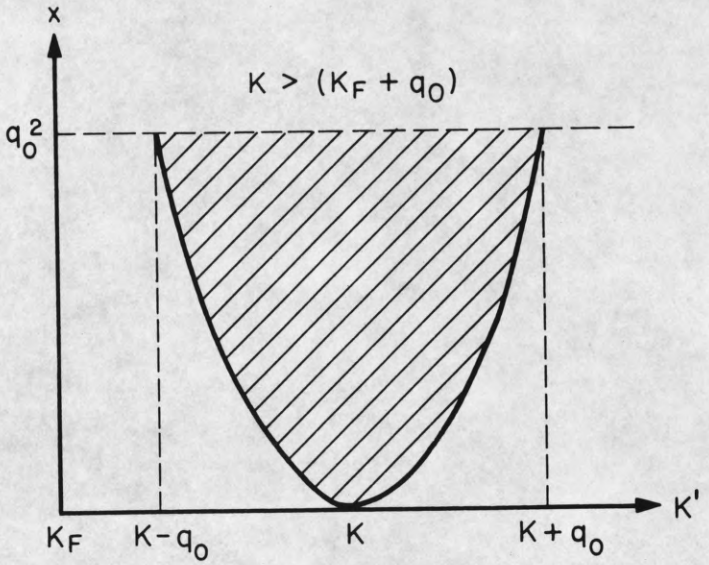

(a)

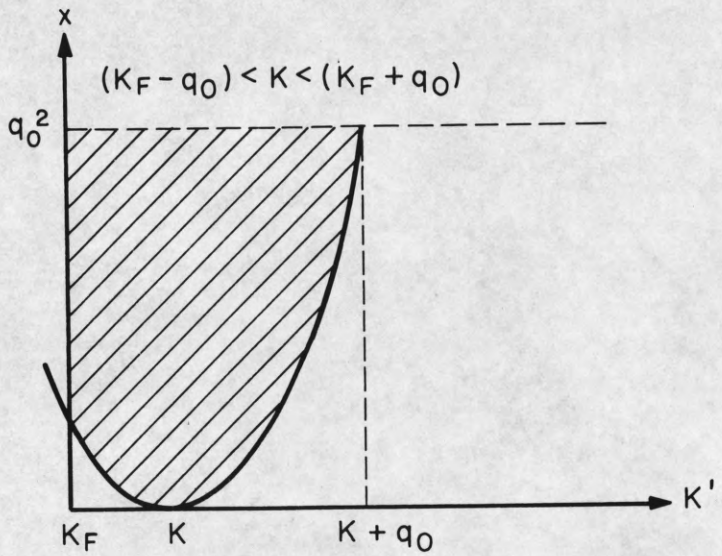

(b)

LR-362

Figure 1

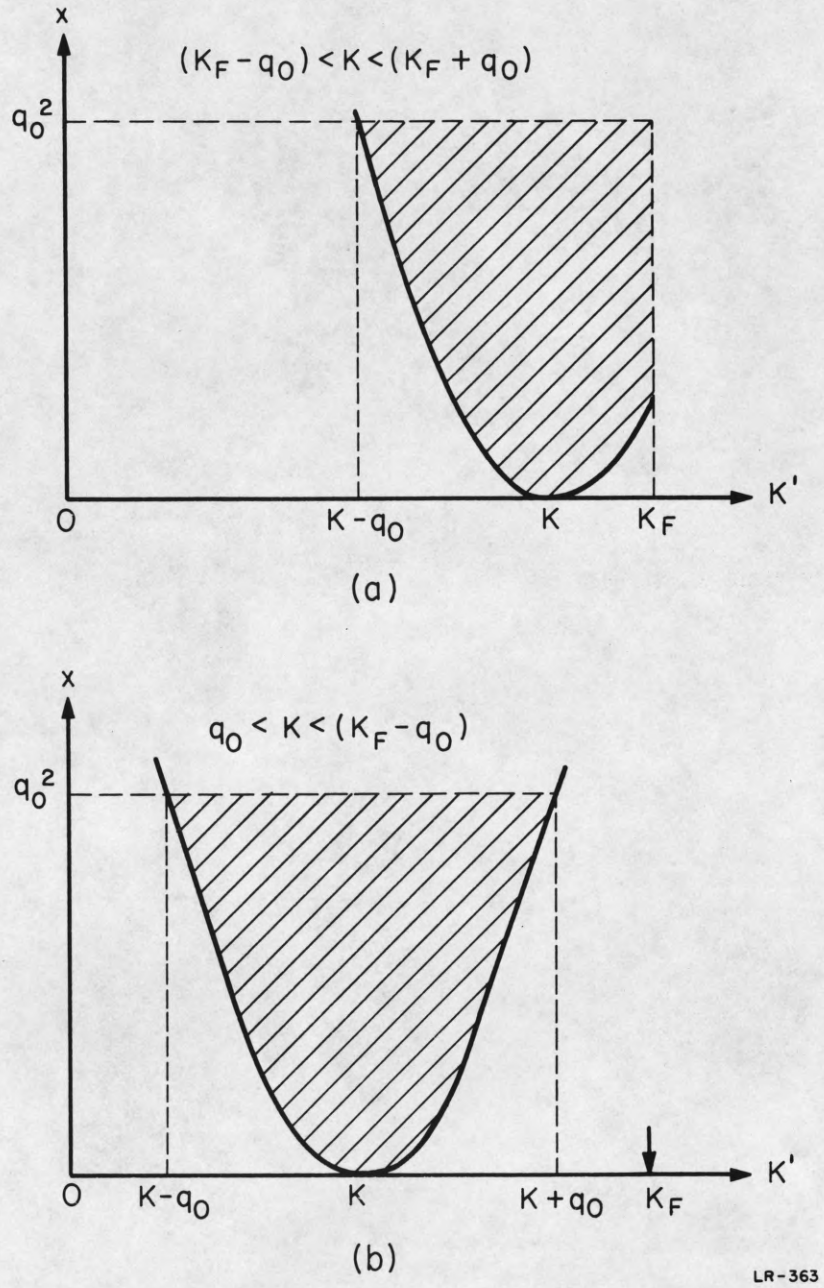
x
$(K_F - q_0) < K < (K_F + q_0)$
q_0^2
O
$K - q_0$
K
K_F
K'
(a)
x
$q_0 < K < (K_F - q_0)$
q_0^2
O
$K - q_0$
K
$K + q_0$
K_F
K'
(b)
LR-363

Figure 2

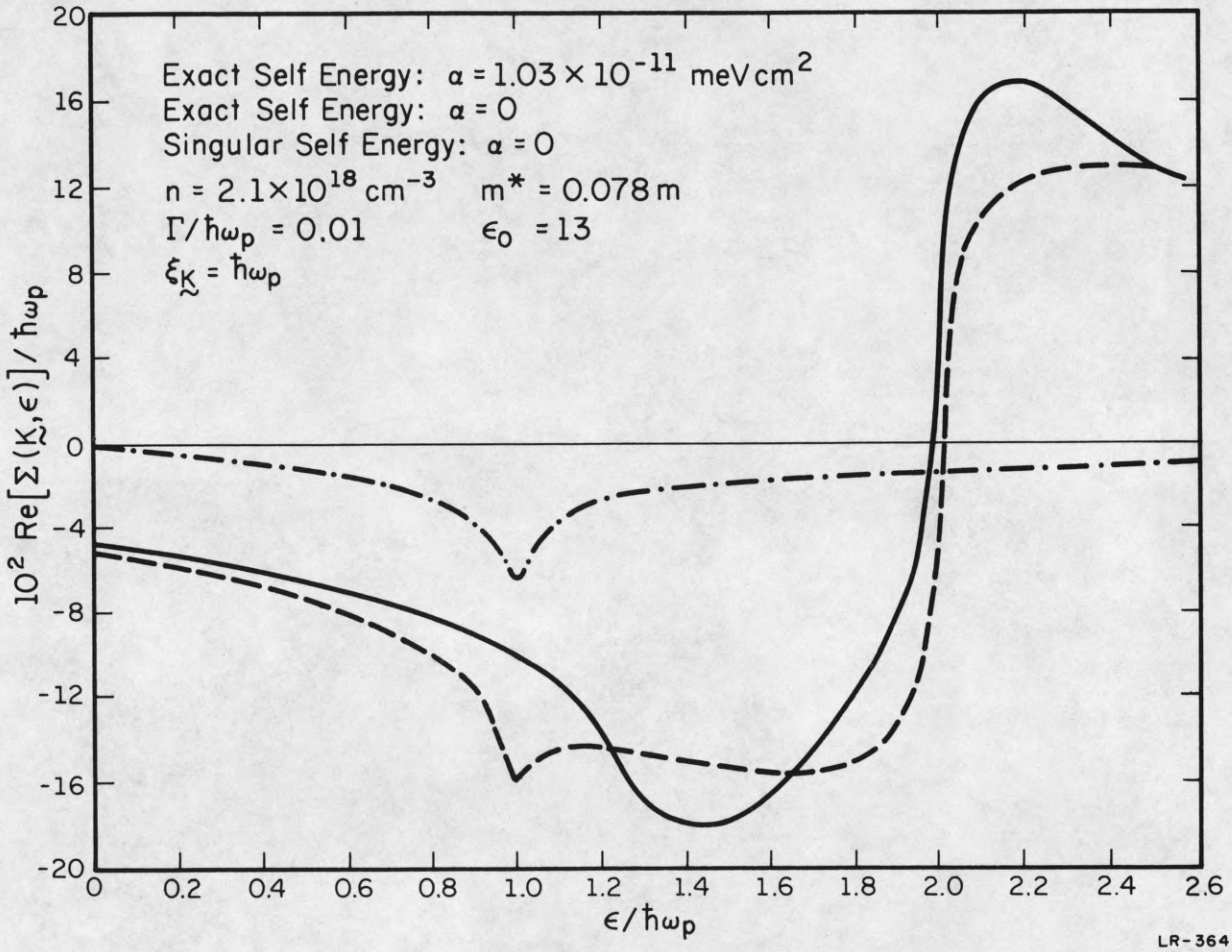
Exact Self Energy: $\alpha = 1.03 \times 10^{-11}$ meV cm^2
Exact Self Energy: $\alpha = 0$
Singular Self Energy: $\alpha = 0$
$n = 2.1 \times 10^{18}$ cm^{-3} $m^* = 0.078\,m$
$\Gamma/\hbar\omega_p = 0.01$ $\epsilon_0 = 13$
$\xi_{\underset{\sim}{K}} = \hbar\omega_p$
$10^2\,\mathrm{Re}[\Sigma(\underset{\sim}{K},\epsilon)]/\hbar\omega_p$
$\epsilon/\hbar\omega_p$
20
16
12
8
4
0
-4
-8
-12
-16
-20
0
0.2
0.4
0.6
0.8
1.0
1.2
1.4
1.6
1.8
2.0
2.2
2.4
2.6
LR-364

Figure 3

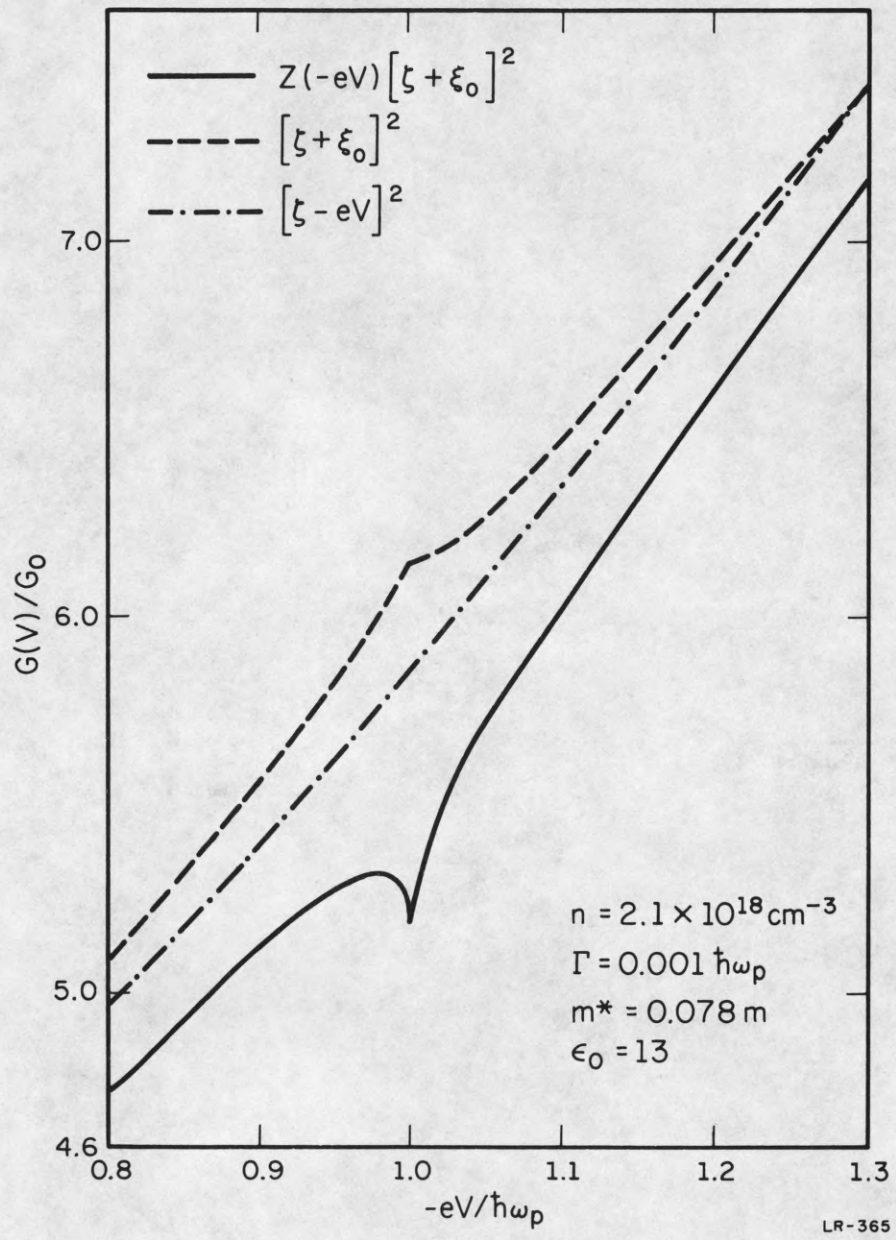
$Z(-eV)\left[\zeta+\xi_0\right]^2$
$\left[\zeta+\xi_0\right]^2$
$\left[\zeta-eV\right]^2$
7.0
6.0
5.0
4.6
G(V)/G₀
0.8
0.9
1.0
1.1
1.2
1.3
-eV/ħω_p
n = 2.1 × 10^18 cm^-3
Γ = 0.001 ħω_p
m* = 0.078 m
ε₀ = 13
LR-365

Figure 4

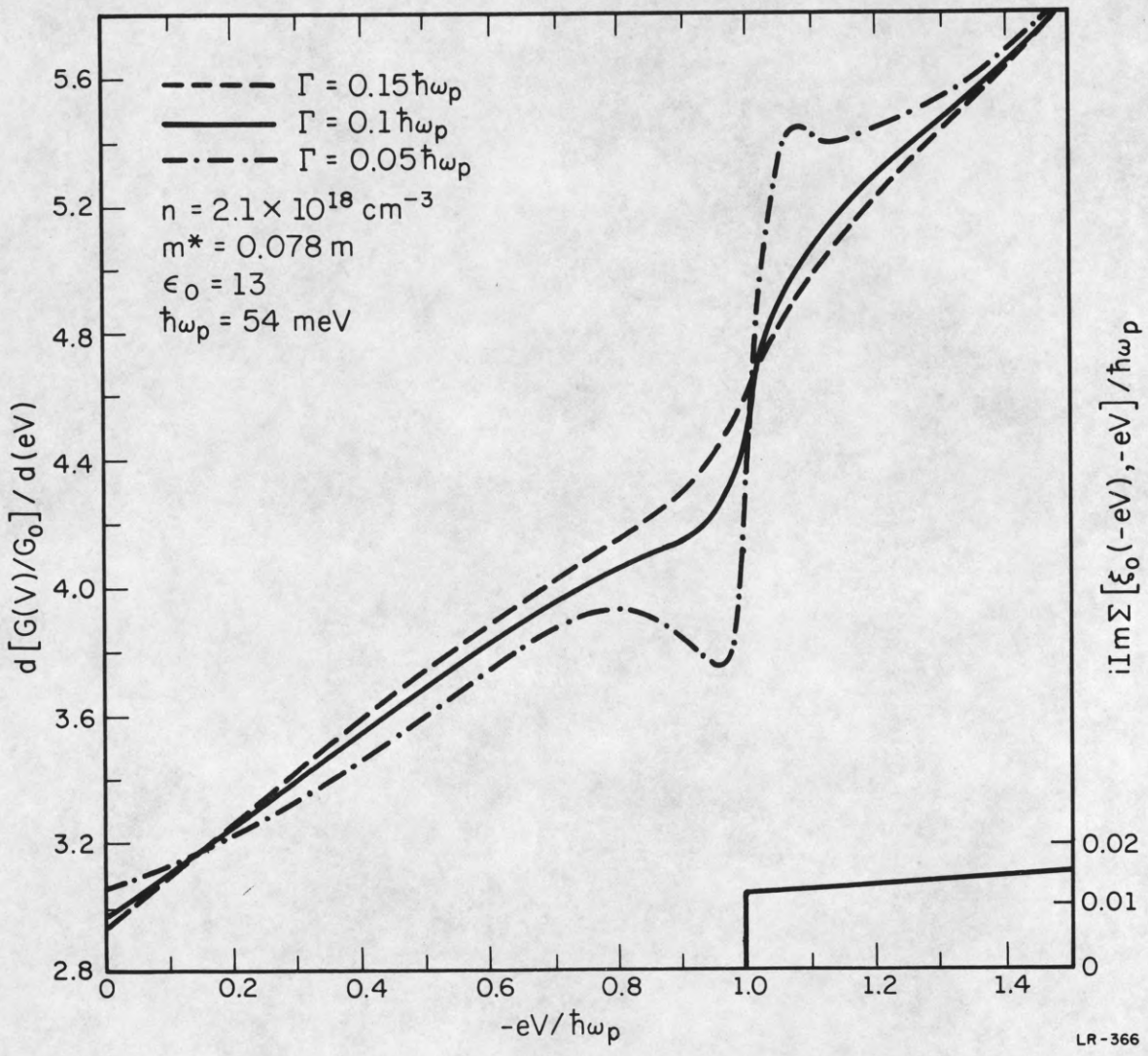
Γ = 0.15ħω_p
Γ = 0.1ħω_p
Γ = 0.05ħω_p
n = 2.1 × 10^18 cm^-3
m* = 0.078 m
ε_0 = 13
ħω_p = 54 meV
d[G(V)/G_0] / d(eV)
-eV/ħω_p
i Im Σ [ξ_0(-eV), -eV] / ħω_p
LR-366

Figure 5

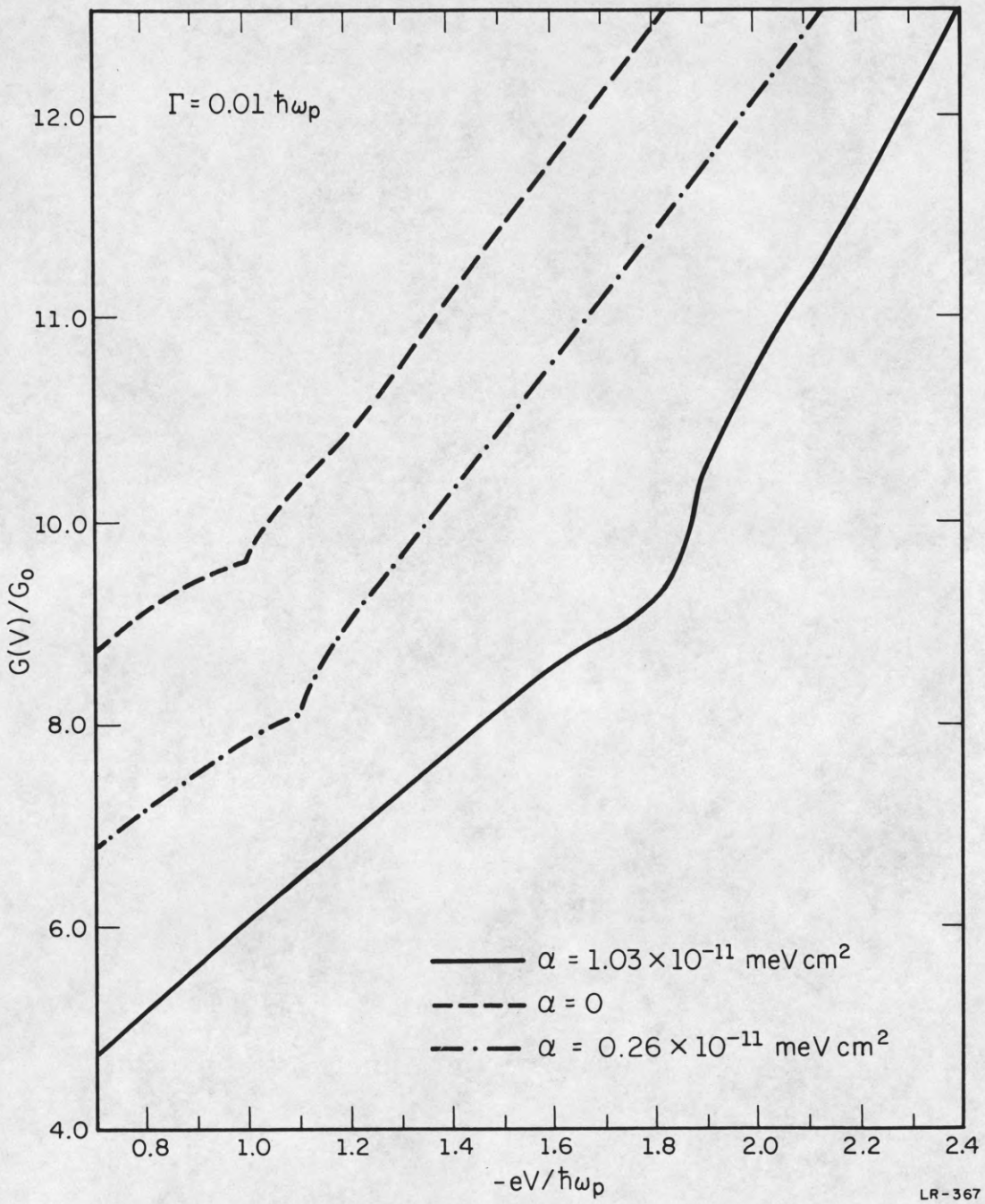
Γ = 0.01 ħω_p
12.0
11.0
10.0
8.0
6.0
4.0
G(V)/G_o
0.8
1.0
1.2
1.4
1.6
1.8
2.0
2.2
2.4
-eV/ħω_p
α = 1.03 × 10^-11 meV cm^2
α = 0
α = 0.26 × 10^-11 meV cm^2
LR-367

Figure 6

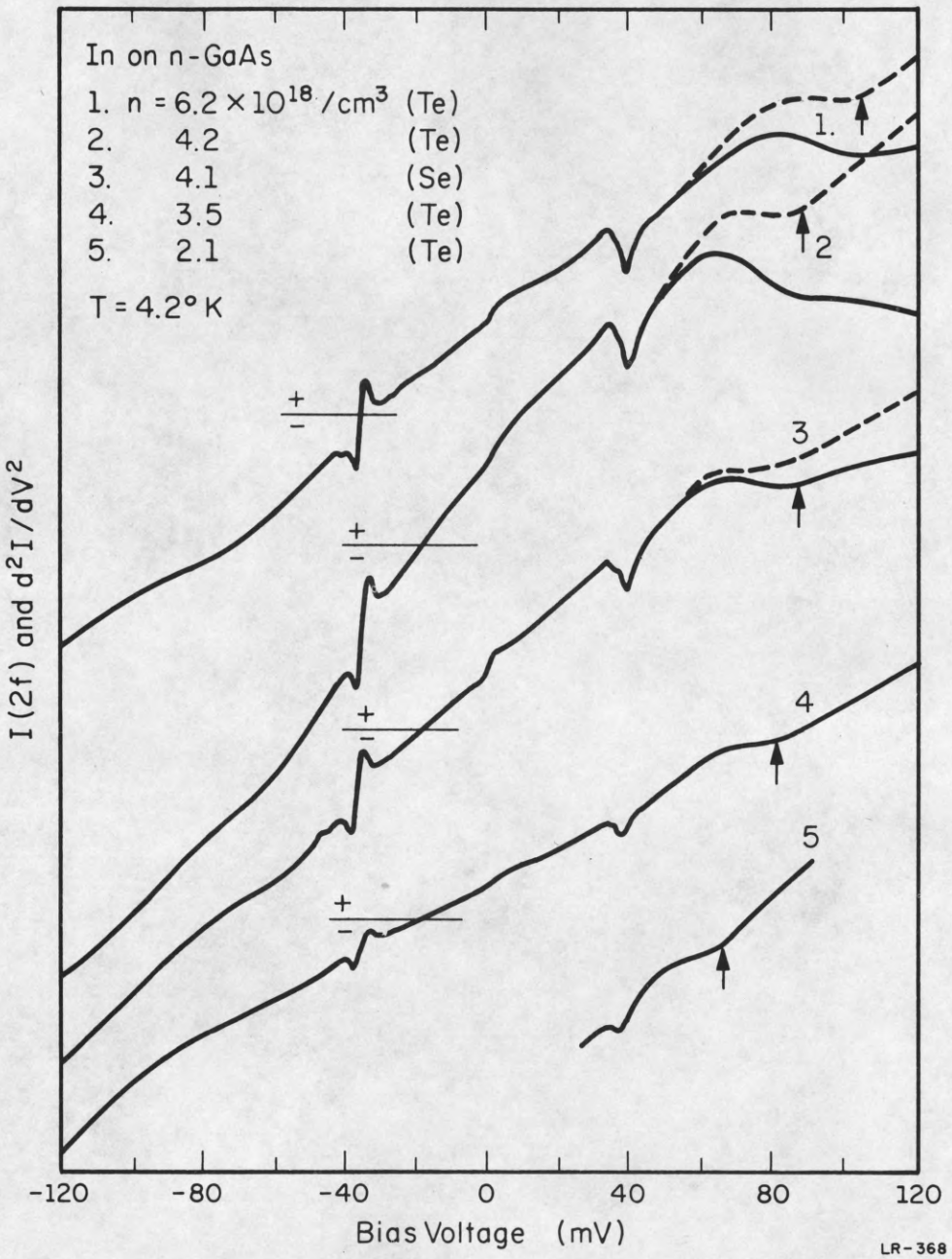
In on n-GaAs
1. n = 6.2 × 10^18 /cm^3 (Te)
2. 4.2 (Te)
3. 4.1 (Se)
4. 3.5 (Te)
5. 2.1 (Te)
T = 4.2° K
I(2f) and d²I/dV²
-120
-80
-40
0
40
80
120
Bias Voltage (mV)
LR-368

Figure 7

Distribution List as of April 1, 1969

Dr A.A. Dougal
Asst Director (Research)
Ofc of Defense Res & Eng
Department of Defense
Washington, D.C. 20301

Office of Deputy Director
(Research and Information, Rm 3D1037)
Department of Defense
The Pentagon
Washington, D.C. 20301

Director, Advanced Research Projects
Agency
Department of Defense
Washington, D.C. 20301

Director for Materials Sciences
Advanced Research Projects Agency
Department of Defense
Washington, D.C. 20301

Headquarters
Defense Communications Agency (340)
Washington, D.C. 20305

Defense Documentation Center
Attn: DDC-TCA
Cameron Station
Alexandria, Virginia 22314 (50 Copies)

Director
National Security Agency
Attn: TDL
Fort George G. Meade, Maryland 20755

Weapons Systems Evaluation Group
Attn: Colonel Blaine O. Vogt
400 Army-Navy Drive
Arlington, Virginia 22202

Central Intelligence Agency
Attn: OCR/DD Publications
Washington, D.C. 20505

Hq USAF (AFRDD)
The Pentagon
Washington, D.C. 20330

Hq USAF (AFRDDG)
The Pentagon
Washington, D.C. 20330

Hq USAF (AFRDSD)
The Pentagon
Washington, D.C. 20330

Colonel E.P. Gaines, Jr.
ACDA/FO
1901 Pennsylvania Ave N.W.
Washington, D.C. 20451

Lt Col R.B. Kalisch (SREE)
Chief, Electronics Division
Directorate of Engineering Sciences
Air Force Office of Scientific Research
Arlington, Virginia 22209

Dr I.R. Mirman
AFSC (SCT)
Andrews Air Force Base, Maryland 20331

AFSC (SCTSE)
Andrews Air Force Base, Maryland 20331

Mr Morton M. Pavane, Chief
AFSC Scientific and Technical Liaison Office
26 Federal Plaza, Suite 1313
New York, New York 10007

Rome Air Development Center
Attn: Documents Library (EMTLD)
Griffiss Air Force Base, New York 13440

Mr H.E. Webb (EMMIIS)
Rome Air Development Center
Griffiss Air Force Base, New York 13440

Dr L.M. Hollingsworth
AFCRL (CRN)
L.G. Hanscom Field
Bedford, Massachusetts 01730

AFCRL (CRMPLR), Stop 29
AFCRL Research Library
L.G. Hanscom Field
Bedford, Massachusetts 01730

Hq ESD (ESTI)
L.G. Hanscom Field
Bedford, Massachusetts 01730 (2 copies)

Professor J. J. D'Azzo
Dept of Electrical Engineering
Air Force Institute of Technology
Wright-Patterson AFB, Ohio 45433

Dr H.V. Noble (CAVT)
Air Force Avionics Laboratory
Wright-Patterson AFB, Ohio 45433

Director
Air Force Avionics Laboratory
Wright-Patterson AFB, Ohio 45433

AFAL (AVTA/R.D. Larson
Wright-Patterson AFB, Ohio 45433

Director of Faculty Research
Department of the Air Force
U.S. Air Force Academy
Colorado Springs, Colorado 80840

Academy Library (DFSLB)
USAF Academy
Colorado Springs, Colorado 80840

Director
Aerospace Mechanics Division
Frank J. Seiler Research Laboratory (OAR)
USAF Academy
Colorado Springs Colorado 80840

Director, USAF PROJECT RAND
Via: Air Force Liaison Office
The RAND Corporation
Attn: Library D
1700 Main Street
Santa Monica, California 90045

Hq SAMSO (SMTTA/Lt Nelson)
AF Unit Post Office
Los Angeles, California 90045

Det 6, Hq OAR
Air Force Unit Post Office
Los Angeles, California 90045

AUL3T-9663
Maxwell AFB, Alabama 36112

AFETR Technical Library
(ETV,MU-135)
Patrick AFB,Florida 32925

ADTC (ADBPS-12)
Eglin AFB, Florida 32542

Mr B.R. Locke
Technical Adviser, Requirements
USAF Security Service
Kelly Air Force Base, Texas 78241

Hq AMD (AMR)
Brooks AFB, Texas 78235

USAFSAM (SMKOR)
Brooks AFB, Texas 78235

Commanding General
Attn: STEWS-RE-L, Technical Library
White Sands Missile Range
New Mexico 88002 (2 copies)

Hq AEDC (AETS)
Attn: Library/Documents
Arnold AFS, Tennessee 37389

European Office of Aerospace Research
APO New York 09667

Phsical & Engineering Sciences Division
U.S. Army Research Office
3045 Columbia Pike
Arlington, Virginia 22204

Commanding General
U.S. Army Security Agency
Attn: IARD-T
Arlington Hall Station
Arlington, Virginia 22212

Commanding General
U.S. Army Materiel Command
Attn: AMCRD-TP
Washington, D.C. 20315

Technical Director (SMUFA-A2000-107-1)
Frankford Arsenal
Philadelphia, Pennsylvania 19137

Redstone Scientific Information Center
Attn: Chief, Document Section
U.S. Army Missile Command
Redstone Arsenal, Alabama 35809

Commanding General
U.S. Army Missile Command
Attn: AMSMI-REX
Redstone Arsenal, Alabama 35809

Commanding General
U.S. Army Strategic Communications Command
Attn: SCC-CG-SAE
Fort Huachuca, Arizona 85613

Commanding Officer
Army Materials and Mechanics Res. Center
Attn: Dr H. Priest
Watertown Arsenal
Watertown, Massachusetts 02172

Commandant
U.S. Army Air Defense School
Attn: Missile Science Division, C&S Dept
P.O. Box 9390
Fort Bliss, Texas 79916

Commandant
U.S. Army Command & General Staff College
Attn: Acquisitions, Library Division
Fort Leavenworth, Kansas 66027

Commanding Officer
U.S. Army Electronics R&D Activity
White Sands Missile Range, New Mexico 88002

Mr Norman J. Field, AMSEL-RD-S
Chief, Office of Science & Technology
Research and Development Directorate
U.S. Army Electronics Command
Fort Monmouth, New Jersey 07703

Commanding Officer
Harry Diamond Laboratories
Attn: Dr Berthold Altman (AMXDO-TI)
Connecticut Avenue and Van Ness St N.W.
Washington, D.C. 20438

Director
Walter Reed Army Institute of Research
Walter Reed Army Medical Center
Washington, D.C. 20012

Commanding Officer (AMXRD-BAT)
U.S. Army Ballistics Research Laboratory
Aberdeen Proving Ground
Aberdeen, Maryland 21005

Technical Director
U.S. Army Limited War Laboratory
Aberdeen Proving Ground
Aberdeen, Maryland 21005

Commanding Officer
Human Engineering Laboratories
Aberdeen Proving Ground
Aberdeen, Maryland 21005

U.S. Army Munitions Command
Attn: Science & Technology Br. Bldg 59
Picatinny Arsenal, SMUPA-VA6
Dover, New Jersey 07801

U.S. Army Mobility Equipment Research
and Development Center
Attn: Technical Document Center, Bldg 315
Fort Belvoir, Virginia 22060

Director
U.S. Army Engineer Geodesy,
Intelligence & Mapping
Research and Development Agency
Fort Belvoir, Virginia 22060

Dr Herman Robl
Deputy Chief Scientist
U.S. Army Research Office (Durham)
Box CM, Duke Station
Durham, North Carolina 27706

Richard O. Ulsh (CRDARD-IPO)
U.S. Army Research Office (Durham)
Box CM, Duke Station
Durham, North Carolina 27706

Mr Robert O. Parker, AMSEL-RD-S
Executive Secretary, JSTAC
U.S. Army Electronics Command
Fort Monmouth, New Jersey 07703

Commanding General
U.S. Army Electronics Command
Fort Monmouth, New Jersey 07703
Attention:AMSEL-SC
RD-GF
RD-MT
XL-D
XL-E
XL-C
XL-S (Dr R. Buser)
HL-CT-DD
HL-CT-R
HL-CT-L (Dr W.S. McAfee)
HL-CT-O
HL-CT-I
HL-CT-A
NL-D
NL-A
NL-P
NL-P-2 (Mr D. Haratz)
NL-R (Mr R. Kulinyi)
NL-S
KL-D
KL-E
KL-S (Dr H. Jacobs)
KL-SM (Drs Schiel/Hieslmair)
KL-T
VL-D
VL-F (Mr R.J. Niemela)
WL-D
1 copy to each symbol listed individually addressed

Dr A.D. Schnitzler, AMSEL-HL-NVII
Night Vision Laboratory, USAECOM
Fort Belvoir, Virginia 22060

Dr G.M. Janney, AMSEL-HL-NVOR
Night Vison Laboratory,USAECOM
Fort Belvoir, Virginia 22060

Atmospheric Sciences Office
Atmospheric Sciences Laboratory
White Sands Missile Range
New Mexico 88002

Missile Electronic Warfare,
Technical Area, AMSEL-WT-MT
White Sands Missile Range
New Mexico 88002

Project Manager
Comman Positioning & Navigation Systems
Attn: Harold H. Bahr (AMCPM-NS-TM), Bldg 439
U.S. Army Electronics Command
Fort Monmouth, New Jersey 07703

Director, Electronic Programs
Attn: Code 427
Department of the Navy
Washington, D.C. 20360

Commander
U.S. Naval Security Group Command
Attn: G43
3801 Nebraska Avenue
Washington, D.C. 20390

Director
Naval Research Laboratory
Washington, D.C. 20390
Attn: Code 2027 6 copies
Dr W.C. Hall, Code 7000 1 copy
Dr A. Brodizinsky, Sup.Elec Div. 1 copy

Dr G.M.R. Winkler
Director, Time Service Division
U.S. Naval Observatory
Washington, D.C. 20390

Naval Air Systems Command
AIR 03
Washington, D.C. 20360 2 copies

Naval Ship Systems Command
Ship 031
Washington, D.C. 20360

Naval ship Systems Command
Ship 035
Washington, D.C. 20360

U.S. Naval Weapons Laboratory
Dahlgren, Virginia 22448

Naval Electronic Systems Command
ELEX 03, Room 2046 Munitions Building
Department of the Navy
Washington, D.C. 20360 (2 copies)

Commander
Naval Electronics Laboratory Center
Attn: Library
San Diego, California 92152 (2 copies)

Deputy Director and Chief Scientist
Office of Naval Research Branch Office
1030 Est Gree Street
Pasadena, California 91101

Library (Code2124)
Technical Report Section
Naval Postgraduate School
Monterey, California 93940

Glen A. Myers (Code 52Mv)
Assoc Professor of Elec. Engineering
Naval Postgraduate School
Monterey, California 93940

Commanding Officer and Director
U.S. Naval Underwater Sound Laboratory
Fort Trumbull
New London, Connecticut 06840

Commanding Officer
Naval Avionics Facility
Indianapolis, Indiana 46241

Dr H. Harrison, Code RRE
Chief, Electrophysics Branch
National Aeronautics & Space Admin.
Washington, D.C. 20546

NASA Lewis Research Center
Attn: Library
21000 Brookpark Road
Cleveland, Ohio 44135

Los Alamos Scientific Laboratory
Attn: Report Library
P.O. Box 1663
Los Alamos, New Mexico 87544

Federal Aviation Administration
Attn: Admin Stds Div (MS-110)
800 Independence Ave S.W.
Washington, D.C. 20590

Head, Technical Services Division
Naval Investigative Service Headquarters
4420 North Fairfax Drive
Arlington, Virginia 22203

Commander
U.S. Naval Ordnance Laboratory
Attn: Librarian
White Oak, Maryland 21502 (2 copies)

Commanding Officer
Office of Naval Research Branch Office
Box 39 FPO
New York, New York 09510

Commanding Officer
Office of Naval Research Branch Office
219 South Dearborn Street
Chicago, Illinois 60604

Commanding Officer
Office of Naval Research Branch Office
495 Summer Street
Boston, Massachusetts 02210

Commander (ADL)
Naval Air Development Center
Johnsville, Warminster, Pa 18974

Commanding Officer
Naval Training Device Center
Orlando, Florida 32813

Commander (Code 753)
Naval Weapons Center
Attn: Technical Library
China Lake, California 93555

Commanding Officer
Naval Weapons Center
Corona Laboratories
Attn: Library
Corona, California 91720

Commander, U.S. Naval Missile Center
Point Mugu, California 93041

W.A. Eberspacher, Associate Head
Systems Integration Division
Code 5340A, Box 15
U.S. Naval Missile Center
Point Mugu, California 93041

Mr M. Zane Thornton, Chief
Network Engineering, Communications
and Operations Branch
Lister Hill National Center for
Biomedical Communications
8600 Rockville Pike
Bethesda, Maryland 20014

U.S. Post Office Department
Library - Room 1012
12th & Pennsylvania Ave, N.W.
Washington, D.C. 20260

Director
Research Laboratory of Electronics
Massachusetts Institute of Technology
Cambridge, Massachusetts 02139

Mr Jerome Fox, Research Coordinator
Polytechnic Institute of Brooklyn
55 Johnson Street
Brooklyn, New York 11201

Director
Columbia Radiation Laboratory
Columbia University
538 West 120th Street
New York, New York 10027

Director
Coordinated Science Laboratory
University of Illinois
Urbana, Illinois 61801

Director
Stanford Electronics Laboratories
Stanford University
Stanford, California 94305

Director
Microwave Physics Laboratory
Stanford University
Stanford, California 94305

Director, Electronics Research Laboratory
University of California
Berkeley, California 94720

Director
Electronic Sciences Laboratory
University of Southern California
Los Angeles, California 90007

Director
Electronics Research Center
The University of Texas at Austin
Austin Texas 78712

Division of Engineering and Applied Physics
210 Pierce Hall
Harvard University
Cambridge, Massachusetts 02138

Dr G.J. Murphy
The Technological Institute
Northwestern University
Evanston, Illinois 60201

Dr John C. Hancock, Head
School of Electrical Engineering
Purdue University
Lafayette, Indiana 47907

Dept of Electrical Engineering
Texas Technological College
Lubbock, Texas 79409

Aerospace Corporation
P.O. Box 95085
Los Angeles, California 90045
Attn: Library Acquisitions Group

Proffessor Nicholas George
California Inst of Technology
Pasadena, California 91109

Aeronautics Library
Graduat Aeronautical Laboratories
California Institute of Technology
1201 E. California Blvd
Pasadena, California 91109

The John Hoplins University
Applied Physics Laboratory
Attn: Document Librarian
8621 Georgia Avenue
Silver Spring, Maryland 20910

Raytheon Company
Attn: Librarian
Bedford, Massachusetts 01730

Raytheon Company
Research Division Library
28 Seyon Street
Waltham, Massachusetts 02154

Dr Sheldon J. Wells
Electronic Properties Information Center
Mail Station E-175
Hughes Aircraft Company
Culver City, California 90230

Dr Robert E. Fontana
Systems Research Laboratories Inc.
7001 Indian Ripple Road
Dayton, Ohio 45440

Nuclear Instrumentation Group
Bldg 29, Room 101
Lawrence Radiation Laboratory
University of California
Berkeley, California 94720

Sylvania Electronic Systems
Applied Research Laboratory
Attn: Documents Librarian
40 Sylvan Road
Waltham, Massachusetts 02154

Hollander Associates
P.O. Box 2276
Fullerton, California 92633

Illinois Institute of Technology
Dept of Electrical Engineering
Chicago, Illinois 60616

The University of Arizona
Dept of Electrical Engineering
Tucson, Arizona 85721

Utah State University
Dept Of Electrical Engineering
Logan, Utah 84321

Case Institute of Technology
Engineering Division
University Circle
Cleveland, Ohio 44106

Hunt Library
Carnegie-Mellon University
Schenley Park
Pittsburgh, Pennsylvania 15213

Dr Leo Youns
Stanford Research Institute
Menlo Park, California 94025

School of Engineering Sciences
Arizona State University
Tempe, Arizona 85281

Engineering & Mathmatical Sciences Library
University of California at Los Angeles
405 Hilgred Avenue
Los Angeles, California 90024

The Library
Government Publications Section
University of California
Santa Barbara, California 93106

Carnegie Institute of Technology
Electrical Engineering Department
Pittsburgh, Pennsylvania 15213

Professor Joseph E. Rowe
Chairman, Dept of Electrical Engineering
The University of Michigan
Ann Arbor, Michigan 48104

New York University
College of Engineering
New York, New York 10019

Syracuse University
Dept of Electrical Engineering
Syracuse, New York 13210

Yale University
Engineering Department
New Haven, Connecticut 06520

Airborne Instruments Laboratory
Deerpark, New York 11729

Raytheon Company
Attn: Librarian
Bedford, Massachusetts 01730

Lincoln Laboratory
Massachusetts Institute of Technology
Lexington, Massachusetts 02173

The University of Iowa
The University Libraries
Iowa City, Iowa 52240

Lenkurt Electric Co,Inc
1105 County Road
San Carlos, California 94070
Attn: Mr E.K. Peterson

Philco Ford Corporation
Communications & Electronics Div.
Union Meeting and Jolly Rods
Blue Bell, Pennsylvania 19422

Union Carbide Corporation
Electronic Division
P.O. Box 1209
Mountain View, California 94041

Electromagnetic Compatibility Analysis Center
(ECAC), Attn: ACLP
North Severn
Annapolis, Maryland 21402

Director
U. S. Army Advanced Materiel Concepts Agency
Washington, D.C. 20315

ADDENDUM

Dept of Electrical Engineering
Rice University
Houston, Texas 77001

Research Laboratories for the Eng. Sc.
School of Engineering & Applied Science
University of Virginia
Charlottesville, Virginia 22903

Dept of Electrical Engineering
College of Engineering & Technology
Ohio University
Athens, Ohio 45701

Project MAC
Document Room
Massachusetts Institute of Technology
545 Technology Square
Cambridge, Massachusetts 02139

Lehigh University
Dept of Electrical Engineering
Bethelehem, Pennsylvania 18015

Commander
Test Command (TCDT-E)
Defense Atomic Support Agency
Sandia Base
Albuquerque, New Mexico 87115

ERRATUM

Mr Jerome Fox, Research Coordinator
Polytechnic Institute of Brooklyn
55 Johnson St (Should be 333 Jay St)
Brooklyn, N.Y. 11201

Security Classification

DOCUMENT CONTROL DATA - R & D

(Security classification of title, body of abstract and indexing annotation must be entered when the overall report is classified)

1. ORIGINATING ACTIVITY *(Corporate author)*
University of Illinois
Coordinated Science Laboratory
Urbana, Illinois 61801

2a. REPORT SECURITY CLASSIFICATION
Unclassified

2b. GROUP

3. REPORT TITLE

TUNNELING MEASUREMENT OF ELECTRON-PLASMON INTERACTIONS IN DEGENERATE SEMICONDUCTORS

4. DESCRIPTIVE NOTES *(Type of report and inclusive dates)*

5. AUTHOR(S) *(First name, middle initial, last name)*

DUKE, C. B. , RICE, M. J. , & STEINRISSER, F.

6. REPORT DATE	7a. TOTAL NO. OF PAGES	7b. NO. OF REFS
June 1969	40	43

8a. CONTRACT OR GRANT NO.
DAAB-07-67-C-0199; also NsG 228-62

b. PROJECT NO.

c.

d.

9a. ORIGINATOR'S REPORT NUMBER(S)
R-420

9b. OTHER REPORT NO(S) *(Any other numbers that may be assigned this report)*

10. DISTRIBUTION STATEMENT

This document has been approved for public release and sale; its distribution is unlimited.

11. SUPPLEMENTARY NOTES

12. SPONSORING MILITARY ACTIVITY
Joint Services Electronics Program
thru U. S. Army Electronics Command
Fort Monmouth, New Jersey 07703

13. ABSTRACT

The electronic proper self energy due to electron-plasmon interactions in degenerate semiconductors has been evaluated using the Random Phase Approximation. This self energy together with elementary models of the barrier penetration factor is used to calculate the tunneling characteristics of rectifying metal contacts on the degenerate semiconductors. The calculations predict broad, doping-dependent resonances in d^2I/dV^2 at $|eV|$ approximately equal to the plasmon energy, $\hbar\omega_p$, in the semiconductor. In contrast to the analogous calculations for electron-phonon interactions, the major features of the predicted lineshapes are due to quasiparticle renormalization [i.e., k dependence of the self energy] rather than quasiparticle dispersion [i.e., ϵ dependence of the self energy]. Comparison of the model calculations with experimental data taken using indium contacts on selenium and tellurium doped GaAs, $2.1 \times 10^{18}\ cm^{-3} \leq n \leq 6.2 \times 10^{18}\ cm^{-3}$, show satisfactory agreement between the predicted and observed lineshapes. The resonance structure in the experimental d^2I/dV^2 characteristics is identified independently with the plasmon energy in the GaAs electrode by correlation with the plasma minimum observed in the infrared reflectivity of the samples used in the tunneling measurements.

DD FORM 1 NOV 65 1473

Security Classification

14 KEY WORDS	LINK A		LINK B		LINK C	
	ROLE	WT	ROLE	WT	ROLE	WT
Tunneling						
Semiconductors						
Plasmon						